

Article

Failure Mode and Optimization for MSCSS with LRBs Based on IDA Method

Buqiao Fan *, Xun'an Zhang, Yanjie Xiao , Mustapha Abdulhadi , Xinwei Wang and Muhammad Moman Shahzad 

School of Mechanics, Civil Engineering and Architecture, Northwestern Polytechnical University, Xi'an 710129, China; jiaoping@nwpu.edu.cn (X.Z.); yjxiaoyj@163.com (Y.X.); engineermustapha@yahoo.com (M.A.); wangxw@mail.nwpu.edu.cn (X.W.); m.mominshahzad@mail.nwpu.edu.cn (M.M.S.)

* Correspondence: buqiao@mail.nwpu.edu.cn

Abstract: The mega-sub controlled structure system with laminate rubber bearings is an emerging seismic control system for high-rise buildings. The system is high-order statically indeterminate with numerous failure modes. To study the failure modes of the structural system and further improve its seismic performance, the dynamic equations and the finite element model of the system were established. Ten different ground motions were selected from the Pacific Earthquake Engineering Research Center ground motion database for the incremental dynamic analysis (IDA). Based on the results of the IDA, the weakest failure mode of the system was identified, and its failure path was found. Two schemes were proposed to optimize the weakest failure mode of the system, and the optimization results were compared. The results show that although the IDA curves from different ground motion inputs are diverse, the plastic hinges are all formed on the sub-structures. Failures of the system are caused by either the excessive floor drift or the excessive shear deformation of rubber bearings. By adjusting the locations and parameters of dampers and rubber bearings, the seismic performance of the system can be improved.

Keywords: MSCSS; incremental dynamic analysis; seismic; rubber bearing; high-rise building; mega-frame



Citation: Fan, B.; Zhang, X.; Xiao, Y.; Abdulhadi, M.; Wang, X.; Shahzad, M.M. Failure Mode and Optimization for MSCSS with LRBs Based on IDA Method. *Buildings* **2022**, *12*, 998. <https://doi.org/10.3390/buildings12070998>

Academic Editor: Francesco Ricciardelli

Received: 30 May 2022

Accepted: 7 July 2022

Published: 13 July 2022

Publisher's Note: MDPI stays neutral with regard to jurisdictional claims in published maps and institutional affiliations.



Copyright: © 2022 by the authors. Licensee MDPI, Basel, Switzerland. This article is an open access article distributed under the terms and conditions of the Creative Commons Attribution (CC BY) license (<https://creativecommons.org/licenses/by/4.0/>).

1. Introduction

High-rise buildings are often built in densely populated areas in metropolises. They shape the skyline of cities and symbolize a thriving economy and advanced technology. Because of the economic and cultural value of high-rise buildings, keeping them safe is essential. Due to the slender shape of high-rise buildings, they are flexible and prone to excessive vibration under wind and earthquakes. Extreme vibration can cause structures to collapse. To prevent such a disaster, various solutions are used to suppress the vibration.

Installing tuned mass dampers (TMD) on structures is one of the most common solutions. Many high-rise buildings around the world, such as the Tokyo Skytree in Tokyo, Al Mas Tower in Dubai, and World Financial Center in Shanghai have TMDs installed [1]. The TMD has a significant effect on reducing the discomfort caused by wind vibration, but it has a limited effect on preventing collapse caused by strong earthquakes. The reason is that although the tuning mass in the TMD sometimes weighs hundreds of tons, it is still too light compared to the weight of the entire structure. In most cases, the tuning mass in the TMD only accounts for 3% of the total mass of the structure; however, the best vibration control effect is achieved when the mass ratio is around 50% [2]. Besides installing TMDs, seismic isolation is another method that can mitigate vibrations caused by earthquakes. Laminated rubber bearings (LRB) are normally used as isolators. Structures above the isolators are separated from the ground or other structures below, so the structure above is

less affected by the earthquake. Isolation works best on low-rise buildings with a natural period of less than 1 s but is not as effective on super-high-rise buildings.

The mega-sub configuration, as shown in Figure 1a, is widely used for the design and construction of high-rise buildings. The mega-sub structure (MSS) is a two-level structural system that contains a mega-structure and multiple sub-structures. Each sub-structure has multiple floors that are referred to as sub-floors in this paper. Sub-floors carry the loads of the floor slabs, partitions, occupants, equipment, etc. The mega-structure has several mega-floors. Each sub-structure is built on and carried by the mega-floor. MSS has many advantages. It can achieve high structural rigidity while minimizing the use of structural steel and multiple sub-structures can be constructed in parallel to save construction time. However, since the sub-structures and mega-structure in the MSS are fixedly connected, it is not a vibration-controlled structure.

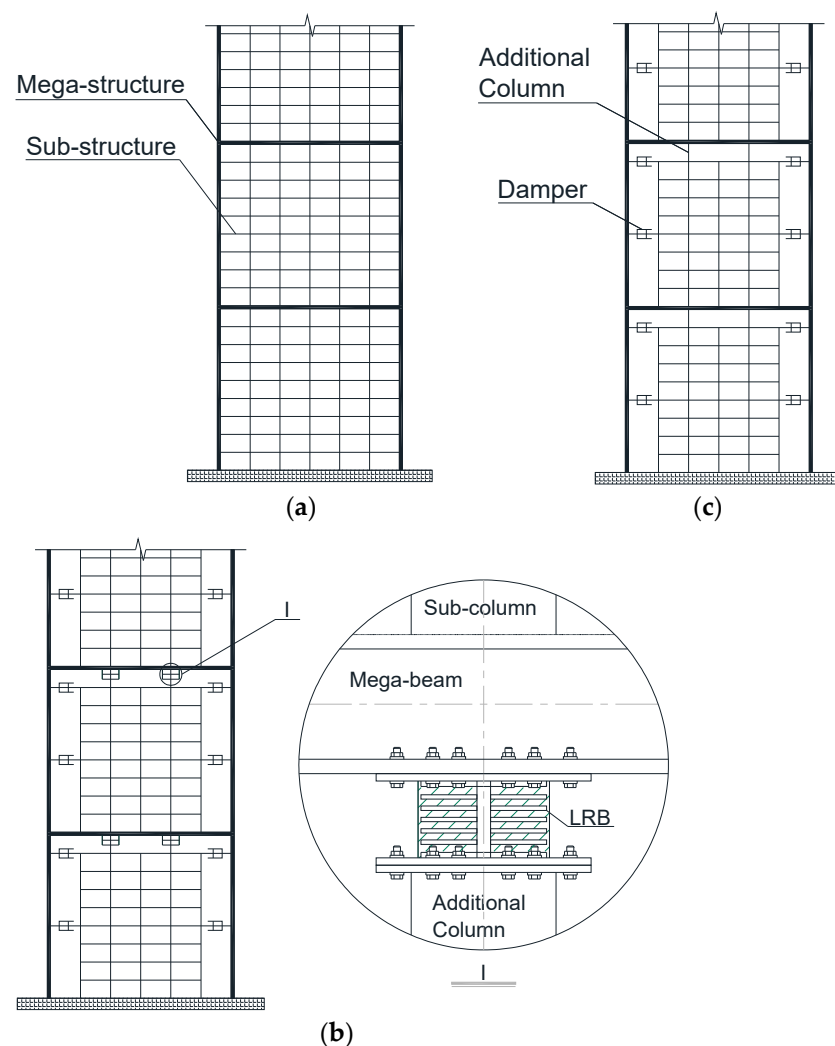


Figure 1. Different structure configurations. (a) MSS without seismic control devices; (b) MSCSS with LRBs [3]; (c) MSCSS without LRBs.

The mega-sub controlled structure system (MSCSS) with LRBs, as shown in Figure 1b, is a new vibration-controlled system. It combines the MSS configuration, LRBs, and the idea of the TMD. It can achieve better seismic performance than the MSS and the traditional MSCSS without LRBs (Figure 1c) [3,4]. In the MSCSS, the sub-structures in the MSS are used as tuning masses. Constraints between the mega-structure and sub-structures in the MSS are replaced by viscous dampers. The relative motion between the main structure and the sub-structure can dissipate the energy input by the earthquake, thereby controlling

the seismic response of the structure. Since the mass ratio of the sub-structure to the main structure can reach 100%, MSCSS performs better than TMD in strong earthquakes [5–7]. Additional columns on sub-structures in the MSCSS can support mega-beams above, reduce bending moments in mega-beams, and allow for larger beam spans. LRBs on additional columns not only dissipate the energy but also further increase the relative motion between the mega-structure and sub-structures, thereby increasing the energy dissipated by the dampers [8–10].

The MSCSS with LRBs has been explored by several researchers. LRBs in the MSCSS can both support the mega-beam above and allow relative motion between the sub-structures and the mega-structure. The relative motion increases the energy dissipation of dampers, and LRBs themselves also dissipate seismic energy, so the kinetic energy and response of the structure will be reduced. Abdulhadi et al. studied the influence of the number, distribution, stiffness, and damping coefficients of dampers and LRBs on the structural response [4] and assessed the fragility of the system to earthquakes [9]. They found that the addition of an LRB at the top of the additional column improves the mechanical behavior. An LRB works well with dampers to reduce the response of the structure. The fragility curve of the MSCSS with LRBs also demonstrates that it has better seismic performance at the moderate and collapse damage limit state. Later, they further investigated the effect of different relative stiffness ratios and mass ratios on the vibration control performance of the sub-structure. The accelerations and displacements of sub-structures in structural systems during earthquakes, and the optimal ranges of relative stiffness ratios and mass ratios were found [10]. Fan et al. developed an optimization program based on a genetic algorithm. Taking the inter-story drift ratio, acceleration, and energy dissipation as optimization objectives, the distribution and parameters of dampers and LRBs in the system were optimized [3]. Fan et al. also proposed the use of structural behavior matrices that are based on the inter-story drift ratio and failure paths as more comprehensive indicators to describe the seismic behavior of MSCSS with LRBs [8]. Yet, there is no investigation on the failure modes of the MSCSS with LRBs. Structural failure is caused by the gradual accumulation of member failures. Different failure types and failure sequences of members lead to different failure modes. The MSCSS with LRBs is high-order statically indeterminate. Its behavior varies greatly under different earthquakes, and it has many failure modes. Obtaining the primary failure mode is essential for improving the seismic performance of the MSCSS with LRBs.

Pushover analysis and incremental dynamic analysis (IDA) are often used to analyze the failure modes of seismic structures. Sun et al. analyzed the failure mode of a high-rise steel-frame structure with the limit state time history analysis and limit state pushover analysis. The seismic capacity of the structure in the governing failure mode was enhanced by progressively strengthening the weakest floors from the bottom floors up, thereby the overall seismic performance of the structure was improved [11]. Bai and Ou identified the weakest failure mode of a reinforced-concrete frame structure [12]. Liu et al. identified the failure modes of multi-span isolated continuous girder bridges based on the weighted rank-sum ratio method [13]. Qiao discussed the failure mode of the rubber bearing of frame-shear foundation isolation structures under near-field impulse earthquakes [14]. In MSCSS with LRBs, the relative motion between the mega-structure and substructures and the hysteresis effects of viscous dampers and LRBs complicate the seismic response of the structure and induce more possible failure modes, but there has been no research on the failure modes of MSCSS with LRBs. In this paper, the dynamic equations of the MSCSS with LRBs are derived. The finite element model was established in ABAQUS. Ground motions from different events and different sites were selected from the Ground Motion Database NGA-West2 of the Pacific Earthquake Engineering Research Center, and IDA was performed on the MSCSS with LRBs. After identifying the failure mode of the structure, the structure was optimized, and the seismic performance of the MSCSS with LRBs was improved.

2. Methods

Incremental dynamic analysis (IDA) is a parametric analysis method used in earthquake engineering. IDA involves scaling seismic records to different intensities, and then using these records of different intensities to perform multiple nonlinear dynamic analyses on the structural model, and record the damage to the structure under each analysis [15–17]. The parameter that measures the intensity of an earthquake is called the intensity measure (IM), and the parameter that measures structural damage is called the damage measure (DM). With IM and DM as the horizontal and vertical axes, the IDA curve can be plotted. This method has been widely used in seismic analysis [18–22].

The selection of ground motion accelerograms has a significant influence on the results of IDA. The accelerograms can be from real seismic events or can be a combination of real and synthetic ones. Haselton et al. and Bazzurro and Cornell suggested that at least seven waves must be used in the analysis to get sufficiently accurate results [23,24]. In this study, ten typical strong earthquake records were selected from the PEER Ground Motion Database NGA-West2 as the ground motion input for the IDA. The ten records are shown in Table 1. RSN in Table 1 stands for the record sequence number, which is a unique number for each ground motion record. Vs30 in the table represents the average shear wave velocity. For the ten selected waves, the average shear wave velocity for the top 30 m of the site is between 360 m/s to 760 m/s, in line with the FEMA450 Class C site [25]. The moment magnitude for all records is above 6.5, and the PGA is between 0.2 g to 1 g. To increase the diversity of the ground motions, records from the same seismic event were avoided. The ten records are from earthquakes that have occurred all over the world. The time interval of all ground motion records is 0.02 s. The duration of all ground motions was cropped to a length of 20 s, leaving the part with the largest acceleration. The acceleration response spectrum and displacement response spectrum of the 10 ground motion records are shown in Figure 2a,b.

Table 1. Selected ground motion records.

| No. | RSN | Earthquake Name | Year | Station Name | Magnitude | Vs30 (m/s) | PGA |
|-----|------|---------------------|------|----------------------------|-----------|------------|--------|
| 1 | 71 | San Fernando, USA | 1971 | Lake Hughes #12 | 6.61 | 602 | 0.3464 |
| 2 | 125 | Friuli-01, Italy | 1976 | Tolmezzo | 6.5 | 505 | 0.3571 |
| 3 | 139 | Tabas, Iran | 1978 | Dayhook | 7.35 | 472 | 0.4094 |
| 4 | 741 | Loma Prieta, USA | 1989 | BRAN | 6.93 | 477 | 0.5023 |
| 5 | 830 | Cape Mendocino, USA | 1992 | Shelter Cove Airport | 7.01 | 519 | 0.2285 |
| 6 | 864 | Landers, USA | 1992 | Joshua Tree | 7.28 | 379 | 0.2840 |
| 7 | 952 | Northridge-01, USA | 1994 | Beverly Hills-12520 Mulhol | 6.69 | 546 | 0.6209 |
| 8 | 1111 | Kobe, Japan | 1995 | Nishi-Akashi | 6.9 | 609 | 0.4832 |
| 9 | 1148 | Kocaeli, Turkey | 1999 | Arcelik | 7.51 | 523 | 0.2101 |
| 10 | 1485 | Chi-Chi, Taiwan | 1999 | TCU045 | 7.62 | 705 | 0.5068 |

There are many studies regarding the selection of the IM, and more than thirty IM indicators have been proposed [15,16,26–29]. The proposed indicators can be divided into two categories: the first includes ground motion indicators such as PGA and peak ground velocity (PGV); the other is the response spectrum indicators, such as the spectral acceleration of the first natural vibration period of the structure. The parameter most widely used as the IM is PGA or the 5% damped spectral response acceleration at the fundamental period of the structure, $S_{aT1,5\%}$. The two indicators are well defined and easy to calculate, but their effectiveness is controversial. For low-level multi-floor structures that are dominated by the first mode, the calculated results are less dispersed when $S_{aT1,5\%}$ is used as the IM; this conclusion is widely supported in the literature [30,31]. For super high-rise buildings, on the other hand, high-order modes also play an important role. It is generally believed that $S_{aT1,5\%}$ is more dispersed than the PGA [28,29]. The MSCSS

with LRBs is designed for high-rise buildings, and the high-order modes have a significant influence on the structure response, so PGA was used as the IM in this research.

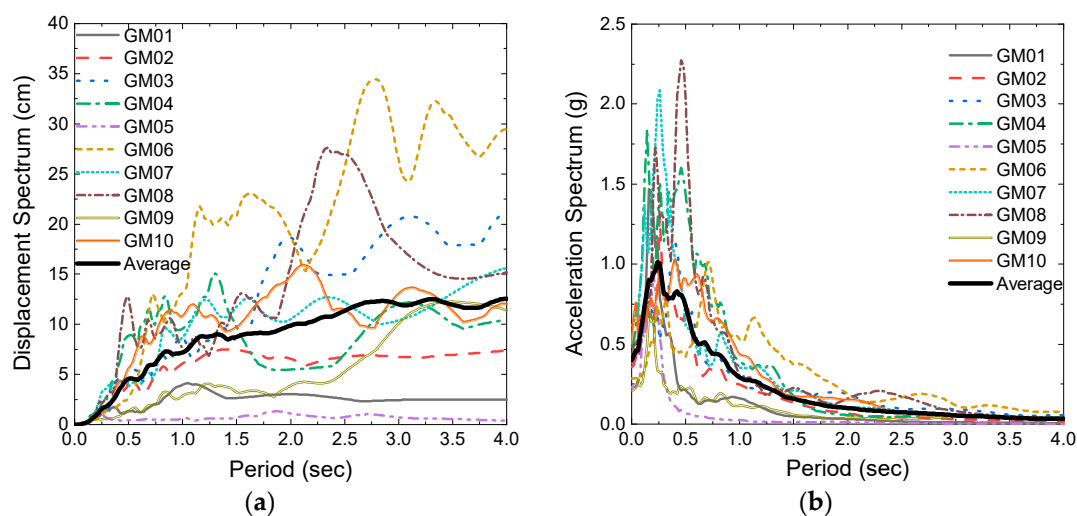


Figure 2. Response spectrum of the selected input ground motions. (a) Displacement response spectrum; (b) acceleration response spectrum.

Whether in real earthquakes or structural model tests, it is rare for structures to remain dynamically stable under earthquakes with a PGA of 5 g. Therefore, the range of the IM on the IDA curve was taken from 0 g to 5 g. The initial increment in PGA for each nonlinear time history analysis was 0.05 g. The accelerograms shown in Table 1 were scaled by multiplying them by a factor. The hunt and fill method proposed by Vamvatsikos [32] was used to reduce unnecessary points on the IDA curve, thereby reducing the number of time history analyses and improving the calculation efficiency. At points where the IDA curve was discontinuous, we reduced the size of the increment to obtain a more refined result. A Python script was used to change the scale of accelerograms at each step of IDA.

The inter-story drift ratio θ was used as the DM, as it is recommended in the FEMA350. The inter-story drift ratio is clearly defined and can be easily determined from the results of linear or nonlinear analyses. It can reliably predict the seismic performance and is closely related to the plastic rotation angle [33]. The inter-story drift ratio θ is defined as the relative displacement between floors divided by floor height. There are mega-floors and sub-floors in the structure. To avoid confusion, θ and the word “drift” in this paper always refer to the sub-floor level drift, even when discussing the drift of the mega-structure.

3. Failure Criteria

Structures respond differently under different ground motions, and there are many possible failure modes of the structure. When one of the failure criteria is met, the structure is considered failed. The MSCSS with LRBs may fail on the structural frame or the LRBs, so the failure criteria can be divided into structural frame failure criteria and LRB failure criteria.

3.1. Structural Frame Failure Criteria

The failure criteria of the structural frame apply to both the mega-frame and the sub-frames. The singularity of the stiffness matrix, excessive deformation, and flattening of the IDA curve are all signs of structural failure. The singularity of the stiffness matrix is the mathematical representation of the instability of the structure. The instability is often caused by the formation of the plastic hinges. As the earthquake intensity increases, so does the number of plastic hinges in the structure. When plastic hinges are formed at some specific locations, the structure will lose stability. For example, when all the columns on the same floor have plastic hinges at both ends, as shown schematically in Figure 3a, the

structure is unstable. Or when the columns form plastic hinges on different floors and the ends of all the restraining beams between them also form plastic hinges, as shown in Figure 3b, the structure is also unstable.

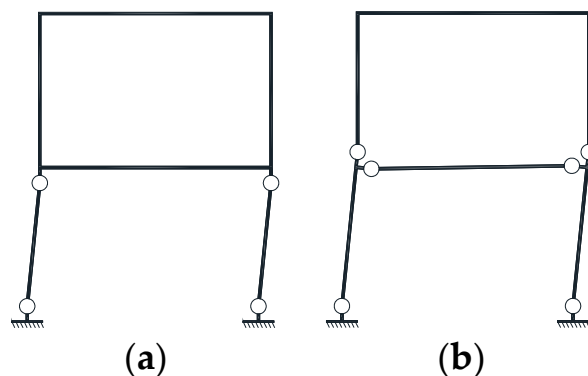


Figure 3. Structural instability caused by plastic hinges: (a) plastic hinges formed at both ends of all the columns on the same floor; (b) plastic hinges formed at different floors on columns and the ends of all the restraining beams.

The deformation of the structure is measured by the inter-story drift ratio. According to the China seismic design code GB50011-2010, when $\theta > 1/50$, high-rise buildings are considered to fail [34].

In most cases, the IDA curve flattens as the IM increases. This phenomenon is called softening. According to FEMA350, when the slope of the line connecting two consecutive points on the individual IDA curve is less than $0.2 S_e$, the structure is considered to fail. S_e is the elastic slope of the IDA curve defined as the slope of the line connecting the origin of the axes to the first point on the curve. When the structure fails, the first of the two consecutive points is considered the ultimate point of the structure.

3.2. LRB Failure Criteria

LRBs in MSCSS are used to reduce the bending moment in the mega-beam. They must have enough vertical stiffness to withstand the massive vertical stress from the structures above. At the same time, to allow relative movements between sub-structures and the mega-structure, LRBs must have a small horizontal stiffness and be able to deform significantly in the horizontal direction. When the vertical stress or horizontal shear deformation exceeds the allowable value, the LRBs on additional columns will be unstable.

The failure criteria of LRBs in this study refer to the seismic design code GB50011-2010. For vertical load in Category B buildings, when the second shape coefficient of the LRB, which is defined as the ratio of effective diameter to total rubber layer thickness, is greater than 5, the vertical compressive stress in the rubber bearing shall be less than 12 MPa, and the vertical tensile stress shall be less than 1 MPa.

The horizontal drift of the LRB shall not exceed the lesser of 0.55 times the effective diameter of the LRB and three times the total thickness of the inner rubber, i.e., $1/\theta_{LRB} \leq \min(0.55D, 3Tr)$. The horizontal drift of the LRB is defined as the displacement between the top and bottom of the LRB.

4. Computational Model

4.1. Lumped Mass Model and Dynamic Equations

The MSCSS with LRBs can be simplified to a lumped mass model as shown in Figure 4. The mass of the mega-structure on each mega-floor is assumed to be concentrated at the roof of the mega-floor, and it is denoted as $m_{p,i}$, where the subscript i is the mega-floor number from 1 to n . The displacement of $m_{p,i}$ relative to the ground is $x_{p,i}$. Similarly, the mass of each sub-floor is assumed to be concentrated at the roof of the sub-floor, and it is denoted as m_{ij} , where j is the sub-floor number from 1 to m . The floors where LRBs and

additional columns are located are also counted as sub-floors, which are colored in black in Figure 4 to distinguish them from other sub-floors. The displacement of the lumped mass of each sub-floor is denoted as x_{ij} . The damping coefficient and stiffness of each sub-floor frame are denoted as c_{ij} and k_{ij} , and the damping coefficient and stiffness of the dampers or LRBs are denoted as $c_{d,ij}$ and $k_{d,ij}$.

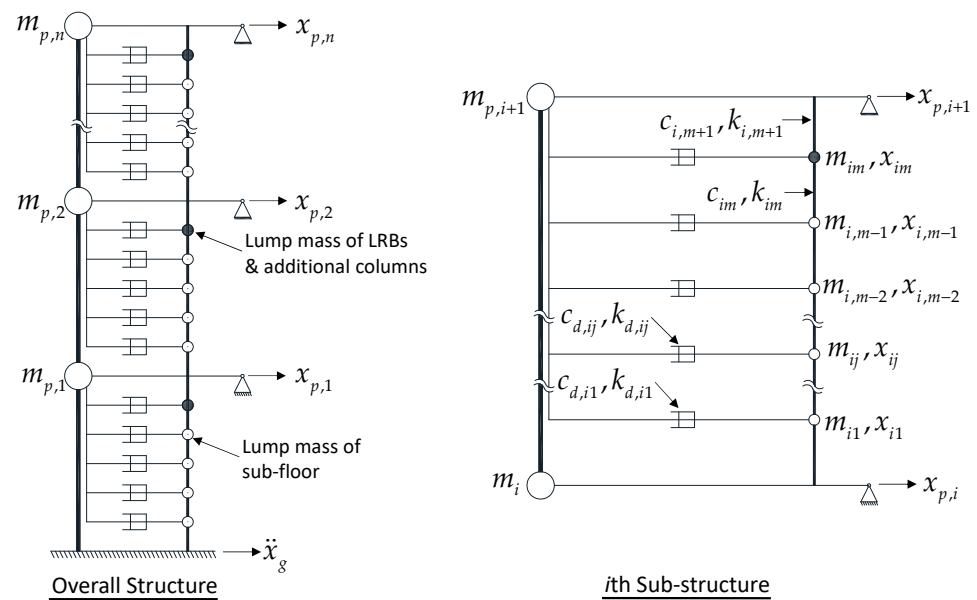


Figure 4. Lumped-mass model for MSCSS with LRBs.

The dynamic equation of the mega-structure can be written as

$$\mathbf{M}_p \ddot{\mathbf{X}}_p + \mathbf{C}_p \dot{\mathbf{X}}_p + \mathbf{K}_p \mathbf{X}_p = -\mathbf{\Gamma} \ddot{x}_g + \mathbf{f} \quad (1)$$

where $\mathbf{M}_p = \text{diag}[m_{p,i}]$, $\mathbf{\Gamma} = \{m_{p,i}\}$, $\mathbf{X}_p = \{x_{p,i}\}$. \mathbf{C}_p and \mathbf{K}_p are the damping and stiffness matrices of the mega-structure. \ddot{x}_g is the ground acceleration. \mathbf{f} is the force exerted on the mega-structure by the sub-structures, and $\mathbf{f} = \{f_i\}$. When $i < n$, f_i can be calculated as follows:

$$f_i = c_{i,m+1}(\dot{x}_{im} - \dot{x}_{p,i}) + k_{i,m+1}(x_{im} - x_{p,i}) + c_{i+1,1}(\dot{x}_{i+1,1} - \dot{x}_{p,i}) + k_{i+1,1}(x_{i+1,1} - x_{p,i}) + \sum_{j=1}^m c_{d,ij}(\dot{x}_{ij} - \dot{x}_{p,i}) + \sum_{j=1}^m k_{d,ij}(x_{ij} - x_{p,i}) \quad (2)$$

When $i = n$, f_i can be calculated as follows:

$$f_n = c_{n,m+1}(\dot{x}_{nm} - \dot{x}_{p,n}) + k_{n,m+1}(x_{nm} - x_{p,n}) + \sum_{j=1}^m c_{d,nj}(\dot{x}_{nj} - \dot{x}_{p,n}) + \sum_{j=1}^m k_{d,nj}(x_{nj} - x_{p,n}). \quad (3)$$

The dynamic equation of the sub-structure can be written as

$$m_{ij} \ddot{x}_{ij} + c_{ij}(\dot{x}_{ij} - \dot{x}_{i,j-1}) + k_{ij}(x_{ij} - x_{i,j-1}) + c_{i,j+1}(\dot{x}_{ij} - \dot{x}_{i,j+1}) + k_{i,j+1}(x_{ij} - x_{i,j+1}) + c_{d,ij}(\dot{x}_{ij} - \dot{x}_{p,i+1}) + k_{d,ij}(x_{ij} - x_{p,i+1}) = -m_{ij} \ddot{x}_g \quad (4)$$

The above dynamic equations can effectively analyze the structure in the elastic stage, but they are not applicable in the plastic stage. Plastic analysis requires the establishment of a finite element model.

4.2. Finite Element Model

The finite element model uses Model III and its optimization results are presented by Fan et al. in [4]. The layout of the structure and section properties are shown in Figure 5. The mega-structure has four mega-floors and is represented by bold lines. Four sub-structures are represented by thin lines, and each has seven sub-floors. The first sub-structure is connected with the mega-structure, while the others are partially released and connected to the mega-structure through viscous dampers, additional columns, and LRBs. The damper and LRB are modeled with the Maxwell viscoelastic model and the Bouc–Wen model, respectively. The damping coefficient and the damping exponent of the damper are 4.5 kN·s/m and 1.4. LRB400 is used. The axial stiffness is 1700 kN/m. Shear stiffnesses before and after yield are 24 kN/m and 2.4 kN/m. The model is 128 m tall and 26 m wide. The heights of the mega-floor and sub-floor are 32 m and 4 m, respectively. The gap between the mega-structure and the released sub-structure is 2.7 m. The sides and the middle beams of the released sub-structures are 4.7 m and 5.6 m. The steel of the frame is Q345 according to Chinese standards.

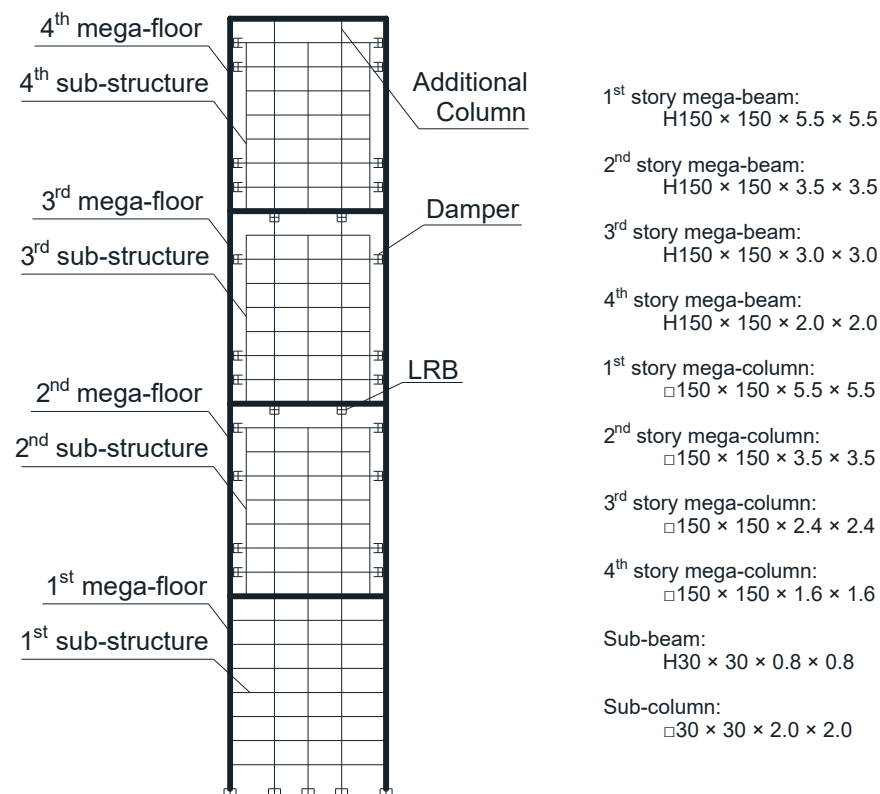


Figure 5. Finite element model of MSCSS with LRBs.

All frames were modeled by beam elements B21 in ABAQUS. Dampers and LRBs were modeled by connector elements CONN2D2, with “axial” connection type for dampers, and “Cartesian + Rotation” for LRBs. By adding inertia non-structure mass, a dead load of 1020 kg/m was applied along the length of beams. The model was submitted to the ABAQUS dynamic implicit solver. Rayleigh damping was used for the structure, and the damping ratio was taken as 0.05. The time history analysis used the fixed 0.02 s increment size.

5. Results and Discussion

5.1. Failure Mode

The IDA curve for the entire structural system and the LRBs are shown in Figure 6a,b. The curves generated under different ground motions are dispersed. The slopes of the curves vary widely, and they exhibit a strong correlation with the displacement response spectra shown in Figure 2a. For instance, at 4 s, which is the natural period of the analyzed model, the displacement response spectrum of GM06 is the highest and that of GM05 is the lowest. These correspond to the curve slopes in Figure 6: GM06 has the smallest slope and GM05 has the largest.

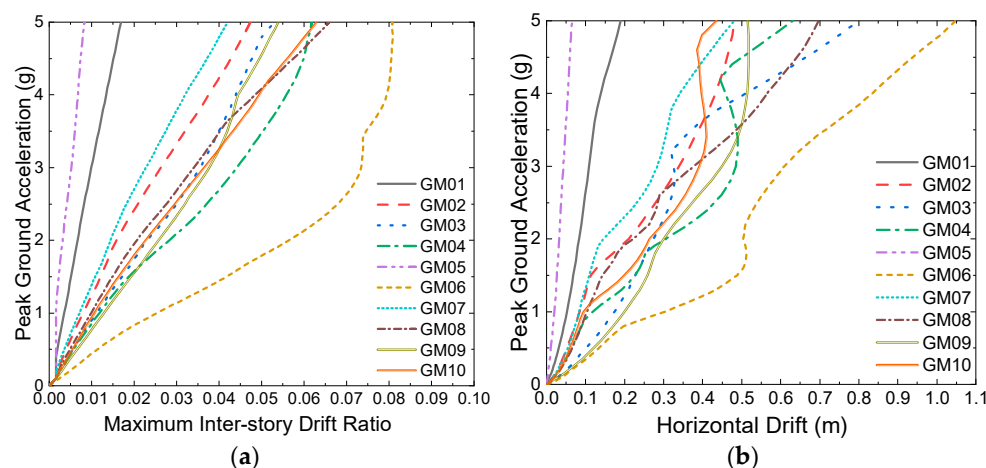


Figure 6. IDA curves under various ground motions: (a) IDA curves for the entire structure; (b) IDA curves for LRBs.

The IDA curves in Figure 6 do not show significant softening. The slopes of curves are always greater than $0.2 S_e$. The softening criterion is never reached. This can be explained by the high flexibility and the long natural period of the structure. The yielding of the structural members has little effect on the value of θ . Some curves even exhibit hardening phenomena, such as GM04 and GM06, and structural resurrection, such as GM04, GM06, and GM10 in Figure 6b.

Figure 7 shows the IDA curves of different parts of the structure. These parts include the four mega-floors and three released sub-structures. The IDA curves intersect each other, indicating that the most deformed location changes with earthquake intensity. The location also varies under different ground motions and is related to the mode of the structure. However, the maximum θ almost always occurs on sub-structures rather than the mega-structure. This is desirable because the mega-structure is the more critical part. Sub-structures are attached to the mega-beams in the mega-structure. The different sub-structures are independent of each other, and the weight of each sub-structure is borne by the mega-structure. The failure of one sub-structure will not cause the rest of the structure to fail, but the collapse of the mega-structure will bring down the entire structure. So, the mega-structure should be stronger than the sub-structures.

Figure 8 shows the maximum inter-story drift ratios on each floor when the 1/50 criterion is reached. Since the criterion is never reached under GM01 and GM05, there are no data for the two ground motions. The shapes of the curves are similar under different ground motions. Drifts are always smaller near the mega-beams and gradually increase with the distance. They are also smaller on the top and bottom mega-floors than on the middle two mega-floors. Drifts on the sub-structure are highly dependent on ground motion. Maximum deformation can occur in any of the three sub-structures.

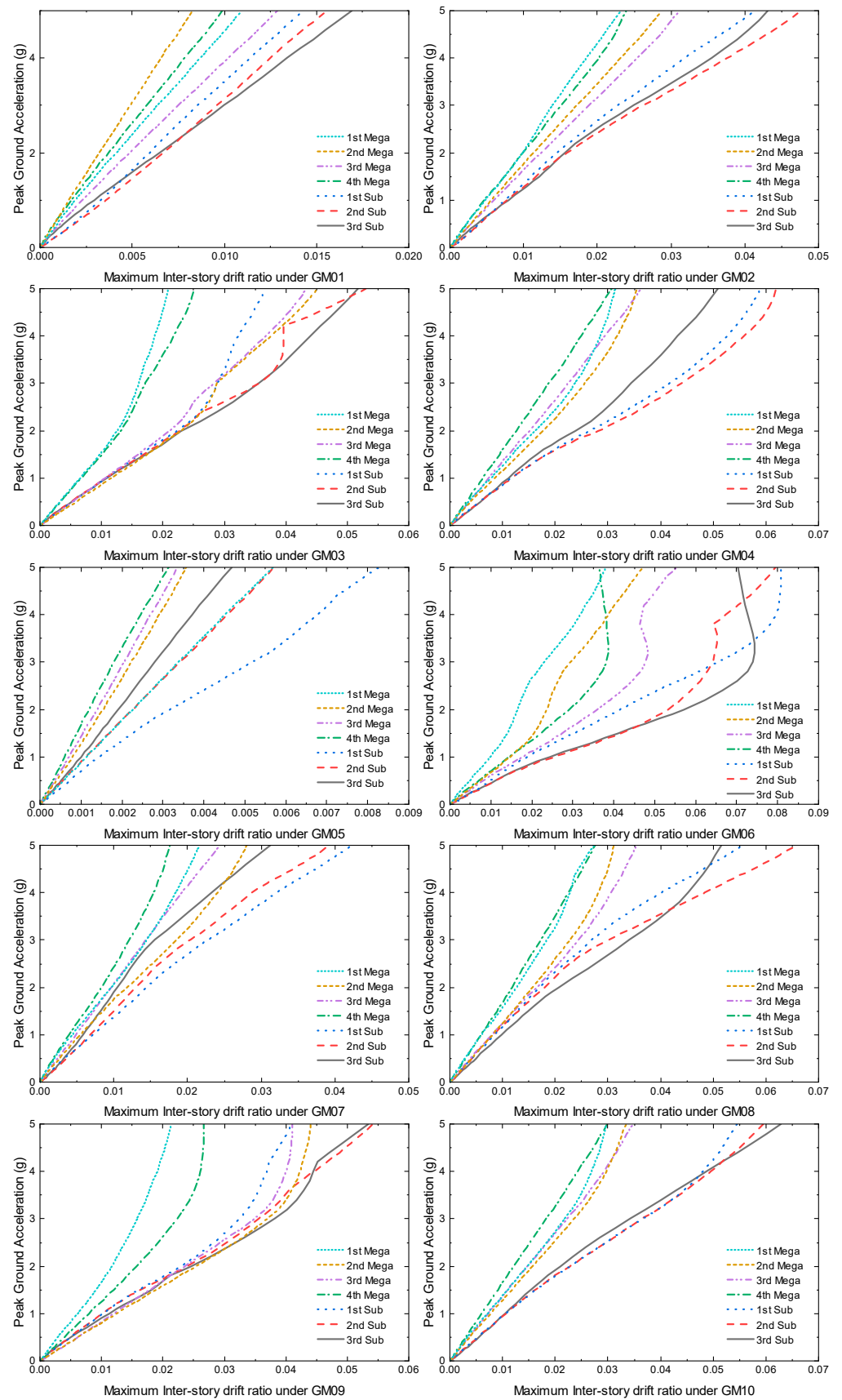


Figure 7. IDA curves for each mega-floor and sub-structure under different ground motions.

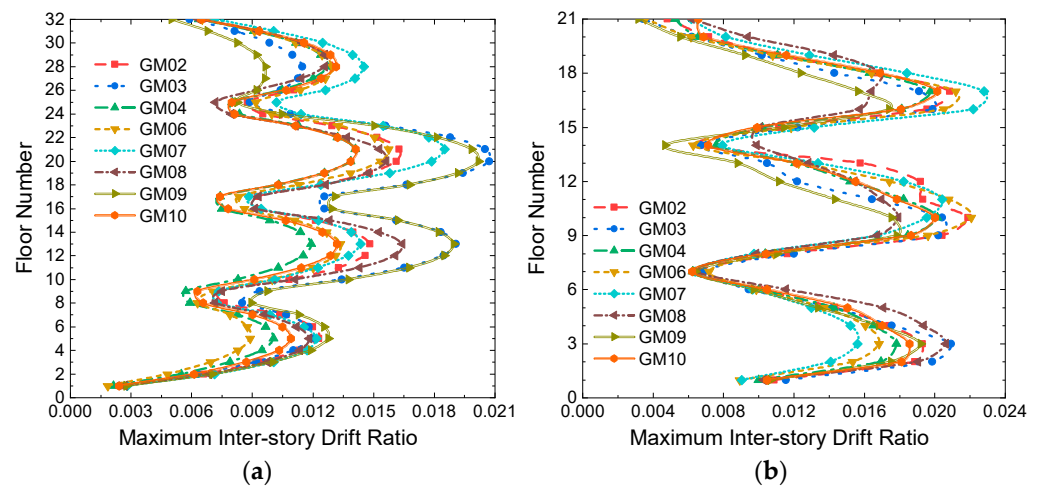


Figure 8. Maximum inter-story drift ratios when the 1/50 criterion is reached. (a) The ratio on each floor in the mega-structure; (b) the ratio on each floor in sub-structures. Vertical axes are sub-floors numbered from the bottom up. Each of the 4 mega-floors includes 8 sub-floors, and each of the 3 released sub-structures includes 7 sub-floors.

The formation of plastic hinges did not destabilize the structure, even when the PGA reached 5 g. The stability failure criterion defined in Section 3 was not exceeded. The governing failure criterion was the floor drift or the horizontal shear deformation of the LRB. The allowable values for the floor drift and the deformation of the LRB were 1/50 and 220 mm. To improve the capacity of the structure, an effort should be made to reduce the floor drift and the shear deformation of LRBs. Table 2 shows the PGA at the allowable values for each ground motion. The structure does not fail under GM01 and GM05, it fails due to excessive drift under GM06 and GM08, and fails due to excessive LRB deformation under the other ground motions. GM06 is the most destructive ground motion with a failure PGA that is much smaller than other records. The shape of the IDA curve of GM06 is also different from the others. The failure mode under the action of GM06 is the weakest.

Table 2. Failure PGA for frame and LRB.

| Ground Motion No. | Failure PGA for Frame (g) | Failure PGA for LRB (g) |
|-------------------|---------------------------|-------------------------|
| GM01 | - | - |
| GM02 | 2.42 | 2.06 |
| GM03 | 1.72 | 1.41 |
| GM04 | 1.59 | 1.46 |
| GM05 | - | - |
| GM06 | 0.83 | 0.84 |
| GM07 | 2.70 | 2.43 |
| GM08 | 1.95 | 1.99 |
| GM09 | 1.59 | 1.15 |
| GM10 | 1.79 | 1.62 |

5.2. Optimization of Structures in Weakest Failure Mode

Figure 9 and Table 3 show the location and sequence of plastic hinge formation under the weakest failure mode. Almost all plastic hinges are formed on sub-beams, and only one is formed on the sub-column. The structure is designed with strong columns and weak beams. The labels in Table 3 indicate member sections. The letter b or c at the beginning of a label represents a sub-beam or a sub-column section. The last letter L or R means that the section is at the left or right end of the beam, and T or B means that it is at the upper or lower end of the column. The three numbers between letters represent the mega-floor number, the sub-floor number, and the number of members counting from left to right. One hundred and seven sections enter the plastic state, and beams on the lower four floors of

released sub-structures all enter the plastic state. The plastic hinges are all formed between 10.02 s and 10.54 s of the earthquake. The drift ratio exceeding 1/50 occurs at 10.36 s, on the third sub-floor of the third sub-structure. The formation of the plastic hinge occurs at almost the same time as the overrun of the drift. The failure of the structure is not due to the accumulation of plastic hinges.

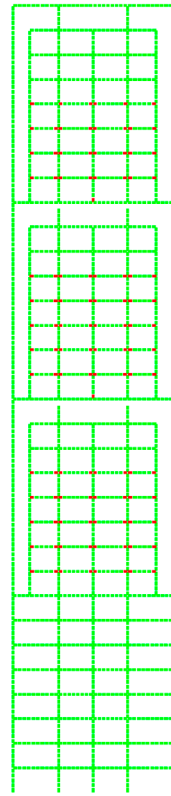


Figure 9. Plastic hinges formed under GM06 at the PGA of 0.83 g.

Table 3. Failure path under GM06 at the PGA of 0.83 g.

| No. | Label |
|-----|-------|-----|-------|-----|-------|-----|-------|-----|-------|-----|-------|-----|-------|
| 01 | b221L | 17 | b234R | 33 | b254R | 49 | b322L | 65 | b344L | 81 | b412R | 97 | b432R |
| 02 | b224R | 18 | b234L | 34 | b321L | 50 | b322R | 66 | b341R | 82 | b413L | 98 | b431R |
| 03 | b211L | 19 | b231L | 35 | b251L | 51 | b334R | 67 | b353L | 83 | b413R | 99 | c413B |
| 04 | b211R | 20 | b231R | 36 | b324R | 52 | b334L | 68 | b353R | 84 | b423L | 100 | b443L |
| 05 | b224L | 21 | b233L | 37 | b314R | 53 | b333L | 69 | b351L | 85 | b423R | 101 | b443R |
| 06 | b214R | 22 | b233R | 38 | b314L | 54 | b333R | 70 | b352L | 86 | b422L | 102 | b442L |
| 07 | b214L | 23 | b232L | 39 | b324L | 55 | b331L | 71 | b352R | 87 | b422R | 103 | b442R |
| 08 | b221R | 24 | b232R | 40 | b321R | 56 | b331R | 72 | b354R | 88 | b433R | 104 | b441L |
| 09 | b213L | 25 | b244R | 41 | b323L | 57 | b332L | 73 | b354L | 89 | b432L | 105 | b444R |
| 10 | b212R | 26 | b241L | 42 | b323R | 58 | b332R | 74 | b351R | 90 | b431L | 106 | b444L |
| 11 | b222L | 27 | b244L | 43 | b311L | 59 | b343L | 75 | b421L | 91 | b414R | 107 | b441R |
| 12 | b222R | 28 | b243L | 44 | b311R | 60 | b343R | 76 | b424R | 92 | b414L | | |
| 13 | b223L | 29 | b243R | 45 | b312L | 61 | b341L | 77 | b424L | 93 | b434L | | |
| 14 | b223R | 30 | b241R | 46 | b312R | 62 | b342L | 78 | b434R | 94 | b411L | | |
| 15 | b213R | 31 | b242L | 47 | b313L | 63 | b342R | 79 | b421R | 95 | b411R | | |
| 16 | b212L | 32 | b242R | 48 | b313R | 64 | b344R | 80 | b412L | 96 | b433L | | |

Based on the above analysis, we first tried to strengthen the structure by increasing the size of weak members. The locations where plastic hinges are formed are the weak points, so the cross-sections of all sub-beams on the lower four floors of released sub-structures were increased from $H30 \times 30 \times 0.8 \times 0.8$ to $H40 \times 30 \times 0.8 \times 0.8$. The criteria

for the increase were to increase the bending resistance of the members and minimize the amount of steel added. The performance of the structure was not improved after the strengthening. The structural response was not reduced but increased. The plastic hinges on the weak sub-beams were not eliminated, but new plastic hinges formed on the original unyielded sub-beams. This phenomenon can be explained by the fact that the stiffened sub-beams attract more stresses that are redistributed from the other part of the structure, thus the original plastic hinges are not eliminated. The increase in stiffness also reduces the relative motion between the mega-structure and the sub-structures, which in turn reduces energy dissipation in the dampers and LRBs and results in greater floor drift and new plastic hinges.

Therefore, we took another approach, which was to increase the energy dissipation of the structure by modifying the locations and parameters of the dampers and LRBs. The studied structure has many possible mounting locations for dampers and LRBs and several parameters that can be adjusted; therefore, the genetic algorithm presented by Fan et al. [3] was applied to optimize the structure. The optimized design variables included the locations of dampers and LRBs, the damping coefficient and exponent of dampers, and the stiffness of LRBs. Maximizing the energy dissipation was set as the objective of the optimization. All design variables were encoded as a 33 digits binary code. The code is a so-called chromosome that represents one possible configuration of the structure. The initial population consisted of 50 randomly generated chromosomes. The fitness of these 50 chromosomes was evaluated based on energy dissipation. Chromosomes with poor fitness were eliminated, and survivors reproduced new chromosomes through crossover and mutation. The probabilities of crossover and mutation were set to 0.8 and 0.02. The results converged in 50 generations. According to the optimization results, the damping coefficient of the damper was adjusted to 4.0 kN · s/cm, and the LRB400 was changed to LRB500. More dampers were added to the roofs of the third floors in the third and fourth sub-structures.

The IDA curves for the original structure and the two modified structures are shown in Figure 10a. The maximum inter-story drift ratios of the three structures are shown in Figure 10b. The PGA, drift ratio, and LRB deformation at failure are reported in numbers in Table 4. It can be seen that strengthening the weak member does not work and should not be used. Increasing the energy dissipation produces the desired result. The failure PGA in the second approach is increased and the maximum inter-story drift ratio is decreased compared to the original structure.

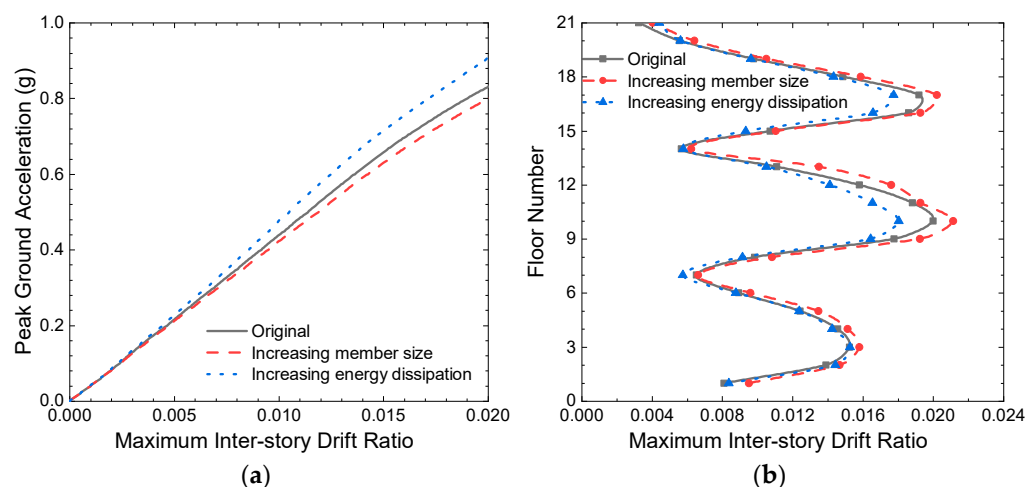


Figure 10. Structure response under GM06 before and after optimization. (a) IDA curve of the structure; (b) maximum inter-story drift ratio of the sub-structures at the 0.83 g PGA.

Table 4. Comparison of the different schemes.

| Structure | PGA (g) | Drift (Rad) | LRB Deformation (mm) |
|-------------------------------|---------|-------------|----------------------|
| Original | 0.83 | 0.02 | 212 |
| Increasing member size | 0.80 | 0.02 | 205 |
| Increasing energy dissipation | 0.91 | 0.02 | 224 |

This was a preliminary study to explore possible factors that can optimize the design. A fully optimized design process should be proposed and this is the likely goal of future papers.

6. Conclusions

In this study, IDA was performed on the MSCSS with LRBs. Ten ground motions from different events were used for the analysis. The structure used for the analysis has 4 mega-floors and 32 sub-floors and was modeled in ABAQUS. The IDA curves of the structure were obtained. The weakest failure mode was identified based on the IDA curve and the failure criteria of the structure. The structure was optimized for the weakest failure mode, and the following conclusions were obtained:

- (1) The IDA curves of the MSCSS with LRBs vary greatly under different ground motion inputs. The maximum inter-story drift ratio is related to the displacement spectrum of ground motions. The failure of the structure is either caused by the excessive drift of sub-floors or the excessive shear deformation of LRBs. The plastic hinges are mainly formed on the ends of sub-beams, which satisfies the “strong column and weak beam” principle.
- (2) Strengthening the yielded weak members cannot improve the seismic performance of the MSCSS with LRBs. The adjustment of the parameters and LRBs of dampers and LRBs can optimize the weakest failure mode and improve the seismic performance of the structure.

Author Contributions: Conceptualization, X.Z. and B.F.; methodology, B.F.; software, B.F.; validation, Y.X., M.A. and X.W.; formal analysis, B.F.; investigation, B.F.; resources, B.F.; data curation, Y.X.; writing—original draft preparation, B.F.; writing—review and editing, B.F., Y.X., M.A., M.M.S. and X.W.; visualization, Y.X.; supervision, X.Z.; project administration, X.Z. All authors have read and agreed to the published version of the manuscript.

Funding: This research received no external funding.

Institutional Review Board Statement: Not applicable.

Informed Consent Statement: Not applicable.

Data Availability Statement: Not applicable.

Conflicts of Interest: The authors declare no conflict of interest.

References

1. Soto, M.G.; Adeli, H. Tuned Mass Dampers. *Arch. Comput. Methods Eng.* **2013**, *20*, 419–431. [[CrossRef](#)]
2. Feng, M.Q.; Mita, A. Vibration Control of Tall Buildings Using Mega Subconfiguration. *J. Eng. Mech.-Asce* **1995**, *121*, 1082–1088. [[CrossRef](#)]
3. Fan, B.; Zhang, X.; Abdulhadi, M.; Wang, Z. Generic Optimization, Energy Analysis, and Seismic Response Study for MSCSS with Rubber Bearings. *Earthq. Struct.* **2020**, *19*, 347–359. [[CrossRef](#)]
4. Abdulhadi, M.; Zhang, X.; Fan, B.; Moman, M. Design, Optimization and Nonlinear Response Control Analysis of the Mega Sub-Controlled Structural System (MSCSS) Under Earthquake Action. *J. Earthq. Tsunami* **2020**, *14*, 2050013. [[CrossRef](#)]
5. Wang, X.; Zhang, X.; Shahzad, M.M.; Wang, T. Research on Dynamic Response Characteristics and Control Effect of Mega-Sub Controlled Structural System under Long-Period Ground Motions. *Structures* **2021**, *29*, 225–234. [[CrossRef](#)]
6. Limazie, T.; Zhang, X.A.; Wang, X.J. Vibration Control Parameters Investigation of the Mega-Sub Controlled Structure System (MSCSS). *Earthq. Struct.* **2013**, *5*, 225–237. [[CrossRef](#)]

7. Zhang, X.A.; Qin, X.J.; Cherry, S.; Lian, Y.D.; Zhang, J.L.; Jiang, J.S. A New Proposed Passive Mega-Sub Controlled Structure and Response Control. *J. Earthq. Eng.* **2009**, *13*, 252–274. [[CrossRef](#)]
8. Fan, B.; Zhang, X.; Abdulhadi, M.; Moman, M.; Wang, Z. Seismic Behavior of MSCSS Based on Story Drift and Failure Path. *Lat. Am. J. SOLIDS Struct.* **2021**, *18*, e411. [[CrossRef](#)]
9. Abdulhadi, M.; Xun'an, Z.; Fan, B.; Moman, M. Evaluation of Seismic Fragility Analysis of the Mega Sub-Controlled Structural System (MSCSS). *J. Earthq. Tsunami* **2020**, *14*, 2050025. [[CrossRef](#)]
10. Abdulhadi, M.; Xun'an, Z.; Fan, B.; Moman, M. Substructure Design Optimization and Nonlinear Responses Control Analysis of the Mega-Sub Controlled Structural System (MSCSS) under Earthquake Action. *Earthq. Eng. Eng. Vib.* **2021**, *20*, 687–704. [[CrossRef](#)]
11. Sun, A.F.; Hou, S.; Ou, J.P. A method for increasing the integral seismic capacity of tall steel buildings based on uniform-damage seismic design. *J. Earthq. Eng. Eng. Vib.* **2012**, *32*, 74–81. [[CrossRef](#)]
12. Bai, J.L.; Ou, J.P. Optimization of failure modes for reinforced concrete buildings based on IDA method. *Eng. Mech.* **2011**, *28*, 198–203.
13. Liu, H.; Tan, P.; Zhang, S.; Zhou, F. Failure Pattern Analysis of an Isolated Continuous Bridge. *J. Sichuan Univ.* **2016**, *48*, 42–49. [[CrossRef](#)]
14. Qiao, Y.B. Study on Arrangement Method and Failure Mode of Rubber Isolation Bearing in Frame—Shear Isolated Structure. Ph.D. Thesis, Lanzhou University of Technology, Lanzhou, China, 2017.
15. Bertero, V.V. Strength and Deformation Capacities of Buildings under Extreme Environments. *Struct. Eng. Struct. Mech.* **1977**, *53*, 29–79.
16. Vamvatsikos, D.; Cornell, C.A. Incremental Dynamic Analysis. *Earthq. Eng. Struct. Dyn.* **2002**, *31*, 491–514. [[CrossRef](#)]
17. Vamvatsikos, D.; Cornell, C.A. Applied Incremental Dynamic Analysis. *Earthq. Spectra* **2004**, *20*, 523–553. [[CrossRef](#)]
18. Christovasilis, I.P.; Filiatrault, A.; Constantinou, M.C.; Wanitkorkul, A. Incremental Dynamic Analysis of Woodframe Buildings. *Earthq. Eng. Struct. Dyn.* **2009**, *38*, 477–496. [[CrossRef](#)]
19. Khorami, M.; Khorami, M.; Alvansazyazdi, M.; Shariati, M.; Zandi, Y.; Jalali, A.; Tahir, M.M. Seismic Performance Evaluation of Buckling Restrained Braced Frames (BRBF) Using Incremental Nonlinear Dynamic Analysis Method (IDA). *Earthq. Struct.* **2017**, *13*, 531–538. [[CrossRef](#)]
20. Lu, D.G.; Yu, X.H.; Wang, G.Y. Structural collapse analysis based on single-record IDA method. *J. Earthq. Eng. Eng. Vib.* **2009**, *29*, 33–39. [[CrossRef](#)]
21. Zhou, Y.; Lu, X.L.; Bo, Y. Application of Incremental Dynamic Analysis to Seismic Evaluation of Hybrid Structure. *J. Tongji Univ.* **2010**, *38*, 183–187+193. [[CrossRef](#)]
22. Zhang, L.X.; Xu, Z.Y.; Liu, J.P.; Zhang, M.Y. Seismic vulnerability analysis of super high-rise hybrid structures based on incremental dynamic analysis. *J. Build. Struct.* **2016**, *37*, 19–25. [[CrossRef](#)]
23. Haselton, C.; Whittaker, A.; Hortacsu, A.; Baker, J.; Bray, J.; Grant, D. Selecting and Scaling Earthquake Ground Motions for Performing Response-History Analyses. In Proceedings of the 15th World Conference on Earthquake Engineering, Lisbon, Portugal, 24–28 September 2012; Earthquake Engineering Research Institute: Oakland, CA, USA, 2012; pp. 4207–4217.
24. Bazzurro, P.; Cornell, C. Seismic Hazard Analysis of Nonlinear Structures .1. Methodology. *J. Struct. Eng.-Asce* **1994**, *120*, 3320–3344. [[CrossRef](#)]
25. FEMA450 NEHRP Recommended Provisions for Seismic Regulations for New Buildings and Other Structures; Building Seismic Safety Council: Washington, DC, USA, 2004.
26. Guan, M.; Du, H.; Cui, J.; Zeng, Q.; Jiang, H. Optimal Ground Motion Intensity Measure for Long-Period Structures. *Meas. Sci. Technol.* **2015**, *26*, 105001. [[CrossRef](#)]
27. Yang, D.X.; Long, H.F. Regressive analysis of intensity parameters of near-fault ground motions and seismic responses of bilinear SDOF systems. *Earthq. Eng. Eng. Dyn.* **2014**, *34*, 9–17. [[CrossRef](#)]
28. Lu, X.; Lu, X.Z.; Ye, L.P.; Li, M.K. Development of an improved ground motion intensity measure for super high-rise buildings. *J. Build. Struct.* **2014**, *35*, 15–21. [[CrossRef](#)]
29. Zhou, Y.; Su, N.F.; Lu, X.L. Study on intensity measure of incremental dynamic analysis for high-rise structures. *J. Build. Struct.* **2013**, *34*, 53–60. [[CrossRef](#)]
30. Vamvatsikos, D.; Fragiadakis, M. Incremental Dynamic Analysis for Estimating Seismic Performance Sensitivity and Uncertainty. *Earthq. Eng. Struct. Dyn.* **2010**, *39*, 141–163. [[CrossRef](#)]
31. Dhakal, R.P.; Mander, J.B.; Mashiko, N. Identification of Critical Ground Motions for Seismic Performance Assessment of Structures. *Earthq. Eng. Struct. Dyn.* **2006**, *35*, 989–1008. [[CrossRef](#)]
32. Vamvatsikos, D. Seismic Performance, Capacity and Reliability of Structures as Seen through Incremental Dynamic Analysis. Ph.D. Dissertation, Stanford University, Stanford, CA, USA, 2002.
33. FEMA350; Recommended Seismic Design Criteria for New Steel Moment-Frame Buildings. Federal Emergency Management Agency: Washington, DC, USA, 2000.
34. GB50011; Code for Seismic Design of Buildings. Ministry of Housing and Urban-Rural Development of the People's Republic of China: Beijing, China, 2010.